Engineering Structures 183 (2019) 135–149

Contents lists available at ScienceDirect

Engineering Structures

journal homepage: www.elsevier.com/locate/engstruct

Experimental research on fire-damaged RC continuous T-beams subsequently strengthened with CFRP sheets

Qingfeng Xu[a,*], Lingzhu Chen[a], Chongqing Han[b], Kent A. Harries[c], Zhimin Xu[b]

[a] Shanghai Key Laboratory of Engineering Structure Safety, Shanghai Research Institute of Building Sciences, Shanghai 200032, China
[b] Architects & Engineers Co., Ltd of Southeast University, Nanjing 210096, China
[c] Department of Civil and Environmental Engineering, University of Pittsburgh, Pittsburgh, PA 15260, USA

ARTICLE INFO

Keywords:
RC continuous T-beam
Temperature distribution
Strengthening
CFRP sheets
Moment redistribution

ABSTRACT

This paper presents experimental results of the structural performance of fire-damaged continuous reinforced concrete (RC) T-beams subsequently strengthened with externally bonded carbon fiber reinforced polymer (EB-CFRP) sheets. A series of seven specimens were tested with different fire exposure time and subsequent strengthening techniques. Experimental results showed that both the unexposed control beams and un-strengthened fire-damaged continuous RC T-beams exhibited flexure failure modes and significant redistribution of moment between hogging and sagging regions. The fire-exposed beams had notably degraded strength and stiffness attributable to the internal temperatures exceeding 500 °C for some portion of the exposure. The EB-CFRP strengthening of fire damaged beams was shown to mostly mitigate the effects of fire exposure. The EB-CFRP retrofit measures successfully restored the virgin capacity of the beam and were sufficient to also restore most of the lost initial stiffness. Simple prediction using plane sections analysis and the assumptions of the 500 °C isotherm method [1] were shown to accurately predict the behaviour of the fire-damaged specimens.

1. Introduction

Elevated temperatures associated with fire exposure cause severe damage to reinforced concrete (RC) structures, resulting in loss of strength and stiffness and the development of relatively large permanent deformations during and following exposure. The behaviours are attributed to the degradation of mechanical properties of both concrete and steel reinforcement and the redistribution of stresses within the beam after fire exposure [2]. Externally bonded carbon fibre reinforced polymer (EB-CFRP) composites are one proposed technique for repairing fire-damaged RC beams. In addition to their acknowledged advantages of having a high strength to weight ratio and good durability [3], EB-CFRP sheets are also easily applied to structures having varying geometry. There exist a number of guide standards for design and installation of EB-CFRP for RC structures – perhaps the most commonly cited is ACI 440.2R-17 [4] which will be referred to in this paper. Countless studies have investigated the flexural behaviour of RC beams strengthened with EB-CFRP sheets under ambient conditions. Results show that EB-CFRP sheets are able to enhance the flexural capacity of beams but decrease the available ductility compared with unstrengthened control beams. Both effects result from the increased effective longitudinal reinforcing ratio afforded by the EB-CFRP. The majority of study on EB-CFRP as a flexural retrofit measure has been conducted on simple span beams and slabs.

In experimental studies of continuous RC beams, improved flexural capacity as a result of the presence of EB-CFRP is reported. However, in continuous beams having discrete EB-CFRP applied in regions of high flexural stress, a primary observed mode of failure is the brittle peeling of the concrete cover at the terminations of the CFRP sheets (so-called “end peel” failure) [5,6]. This failure mode, while simple to mitigate in determinate structures [4], is difficult to address in continuous structures in which there is a stress reversal at the girder faces, the point of inflection is not fixed, and moment redistribution is likely. Aiello et al. [7,8] investigated the ability of RC continuous beams strengthened with CFRP to redistribute moment and found that the percentage of moment redistribution of the analysed beams reaches 20%. ACI 440.2R-17, for instance, permits redistribution up to 20% but also cautions that the redistribution that can be relied upon falls with increasing EB-CFRP reinforcement. The adoption of hybrid (carbon/glass) FRP sheets has been shown to improve the ductility that may be achieved in FRP-repaired continuous RC beams [9].

Although there is considerable research addressing the behaviour of RC beams strengthened with CFRP sheets under ambient conditions, few studies have addressed the repair of heat- and/or fire-damaged RC

* Corresponding author.
E-mail address: xuqingfeng@sribs.com.cn (Q. Xu).

https://doi.org/10.1016/j.engstruct.2019.01.025
Received 22 August 2018; Received in revised form 3 January 2019; Accepted 6 January 2019

Table 1
Details of test specimens.

Beam No.	Standard fire exposure time (min)	Load while exposed to fire	Top (slab) CFRP over the middle support			Bottom (soffit) CFRP along the span		
			Plies	Effective longitudinal reinforcing ratio, ρ_{eff}	Length (m)	Plies	Effective longitudinal reinforcing ratio, ρ_{eff}	Length (m)
GB1	0	–	–	0.0027	–	–	0.0067	–
GB2	0	–	–	0.0027	–	–	0.0067	–
FGB2	60	$0.3P_u$	–	0.0027	–	–	0.0067	–
FGB3	90	$0.3P_u$	–	0.0027	–	–	0.0067	–
SGB1	60	$0.3P_u$	–	0.0027	–	1	0.0076	3.85
SGB2	60	$0.3P_u$	1	0.0031	1.8	1	0.0076	3.85
SGB3	90	$0.3P_u$	–	0.0027	–	2	0.0085	3.85

$\rho_{eff} = \rho_s + \rho_f = A_s/b_w d + (E_f/E_s)A_f/b_w d$.
P_u determined as capacity of control specimens GB1 and GB2.

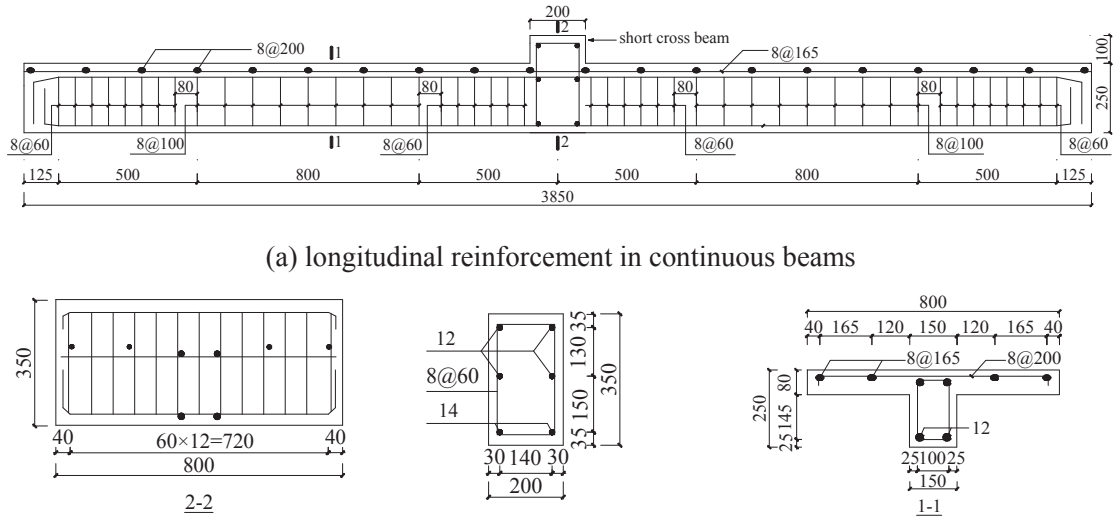

(a) longitudinal reinforcement in continuous beams

(b) reinforcement in the short cross beam at Section 2-2

(c) transverse reinforcement at Section 1-1

Fig. 1. Geometry of continuous RC T-section specimens.

beams. Kumar et al. [10], Haddad et al. [11,12] and Irshidat and Al-Saleh [13] report the effectiveness of externally applied FRP materials at increasing the flexural capacity of heat-damaged simply supported beams. However, in each case, the beams were heated to a specified temperature using an electrical furnace rather than being subject to fire. In addition, as reviewed by Jumaat et al. [14], most of the existing research was conducted on rectangular RC sections which are not representative of typical RC structures that include a composite slab, forming a T-section. This is an important distinction in heat/fire damage since the presence of the slab 'insulates' the upper region of the beam in a typical fire scenario. Xiang et al. [15] and Yu et al. [16] investigated the performance of fire-damaged continuous RC T-beams and slabs strengthened with CFRP sheets. CFRP sheets were shown to effectively recover the strength and stiffness of the continuous beams following fire exposure. In these studies, all CFRP strengthened fire-damaged continuous T-beams exhibited tensile rupture of CFRP sheets. The steel reinforcement in the beams reported by [15] and [16] had a nominal yield strength of 335 MPa; selected to represent the relatively lower strength bars commonly used in older practice. Nonetheless, a design method for EB-CFRP strengthened fire-damaged RC continuous beams is not known in the literature or in existing guide standards.

This paper reports the results of tests on two-span continuous fire-damaged RC T-beams subsequently strengthened with CFRP sheets; a simplified method for calculating their ultimate capacities is also validated.

2. Experimental programme

2.1. Test specimens

Seven large-scale continuous RC T-beams (Table 1) were prepared and tested. All specimens are initially identical and were designed according to the specifications of the Chinese National Code for design of concrete structures [17]. Details of the continuous beam specimens are shown in Fig. 1. The beams are relatively lightly reinforced, having a longitudinal reinforcement ratio $\rho = A_s/b_w d = 0.0067$ in their sagging region and 0.0027 in the hogging region. Control Specimens GB1 and GB2 (replicate specimens) were tested to failure at ambient temperature to obtain the ultimate capacity of the beams. The remaining five specimens were exposed to an ISO 834 [18] standard fire prior to continued testing. Specimens FGB2 and FGB3 were tested to failure without any repair measures – including the removal of fire-damaged

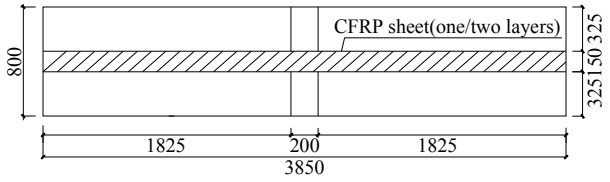

(a) bottom CFRP sheets along the spans of SGB1~SGB3

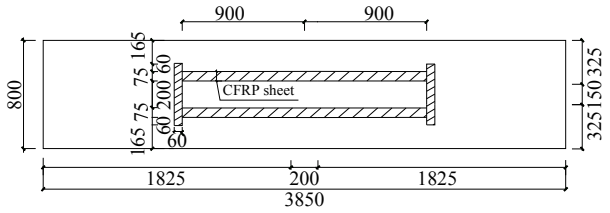

(b) top CFRP sheets over the middle support of SGB2

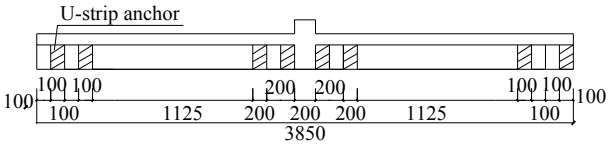

(c) U-strip anchors

Fig. 2. Arrangement of EB-CFRP sheets.

cover concrete – following exposure to the standard fire for 60 and 90 min, respectively. Specimens SGB1 ~ SGB3 were repaired and strengthened with different arrangement of CFRP sheets following exposure to the standard fire for 60 or 90 min, and then loaded to failure. Specimen SGB1 (Fig. 2a) was strengthened with one ply of EB-CFRP at the bottom face (soffit) of the beam along the whole span following 60 min standard fire exposure. Specimen SGB2 was the same as SGB1 except for the additional provision of one ply EB-CFRP over the middle support (top of slab) as shown in Fig. 2b. Specimen SGB3 was strengthened with two plies of EB-CFRP sheets at the bottom face along the whole span following 90 min standard fire exposure. In all cases, the width of the bottom CFRP sheet was the same as the width of the girder stem: 150 mm (Fig. 2a). CFRP U-strip anchors, shown in Fig. 2c, were installed at each side support and at the middle support, to prevent premature peeling of the CFRP sheets. On the top surface of Specimen SGB2, two 75 mm wide and 1800 mm long EB-CFRP sheets were bonded at a distance of 200 mm (this replicates the need for the CFRP to be arranged outside of a column that would typically be at this location. These CFRP sheets were anchored with short CFRP strips as shown in Fig. 2b. A summary of specimen test parameters is provided in Table 1. As can be seen, the application of EB-CFRP increases the effective reinforcing ratio in the sagging region considerably (about 14% per ply).

Since the specimens must span the furnace, the middle support of specimens was inside the furnace exposed to fire directly. To permit the measurement of reaction force at the middle support (using force transducers outside the furnace) and to avoid effects of potential failure of the middle support, the middle support was suspended (anchored outside the furnace) as shown in Fig. 3(c), an approach successfully demonstrated previously [19].

2.2. Material properties

All specimens were cast with commercial ready-mix concrete having siliceous coarse aggregate. The measured cube compressive strength of concrete at ambient temperature at 28 days was 64.5 MPa, and the elastic modulus was 35,800 MPa. Table 2 lists the measured materials properties of the steel reinforcement used. The wet layup CFRP sheets used at an areal weight of 305 g/m^2 and a design thickness of 0.167 mm. The manufacturer-reported ultimate tensile strength and tensile elastic modulus were 3540 MPa and 242,000 MPa, respectively, making the rupture strain 0.0146. Thus, as noted above, the effective additional reinforcement area provided by a single ply 150 mm wide strip of CFRP is: $A_f = (E_f/E_s)t_f b_f = (242/200) \times 0.167 \times 150 = 30.3$ mm^2 steel equivalent (the equivalent of a single 6.2 mm diameter bar). The manufacturer-reported tensile strength, tensile elastic modulus, elongation, and CFRP-to-concrete tensile bond strength of the epoxy resin used was 50.5 MPa, 2600 MPa, 1.58% and 2.9 MPa, respectively.

2.3. EB-CFRP repair method

Prior to EB-CFRP repair of SGB1, SGB2 and SGB3, severely fire-damaged concrete was first removed manually with a hammer and coarse aggregate exposed; the thickness of the removed fire-damaged concrete was about 10 mm for SGB1 and SGB2, 25 mm for SGB3 respectively. The relatively minor damage to SGB1 and SGB2 was made smooth using epoxy resin. For the more sever cover damage to SGB3, the original cross section was restored using high performance shrinkage compensating grout. The resulting surfaces were smoothed and leveled using a diamond grinding disk and cleaned using a vacuum prior to applying the EB-CFRP sheets. The EB-CFRP sheets were cut to length and width and saturated in a resin bath before being applied to the concrete surface using a roller to ensure a smooth application and no air pockets. U-strip anchors were placed in the same manner prior to the initial cure of the longitudinal CFRP strips. Careful preparation and repair of the concrete surface before EB-CFRP repair is necessary to improve the strengthening effect of CFRP sheets; guides such as [4] provide minimum requirements for achieving a sound substrate.

2.4. Fire-exposure

The fire-exposure experiments were carried out in a horizontal furnace with the test setup shown in Fig. 3. The age of concrete during fire-exposure experiments was 60 days. Five specimens were exposed to fire for either 60 min or 90 min, with the furnace temperature programmed to follow the ISO 834 standard fire curve [18]. As shown in Fig. 4, the furnace temperature matched the standard curve very well. Specimens were cooled to ambient temperature following heating. During the fire exposure and for 180 min thereafter, a 41 kN load was applied at the middle of each (sagging) span as shown in Fig. 3. This load was selected as being 30% of the average ultimate load of the control specimens GB1 and GB2. The load was distributed evenly across the 800 mm width of the concrete slab using steel spreader beam laid below the loading jack. The tension in the middle rod (hogging region) required to maintain the condition of no deflection at this point relative to the end supports was 56.4 kN. The actual applied loads and reactions were recorded with load transducers placed at each support and each load point. Displacement transducers (LVDTs) were attached to the supports and the load points to monitor the vertical displacements at

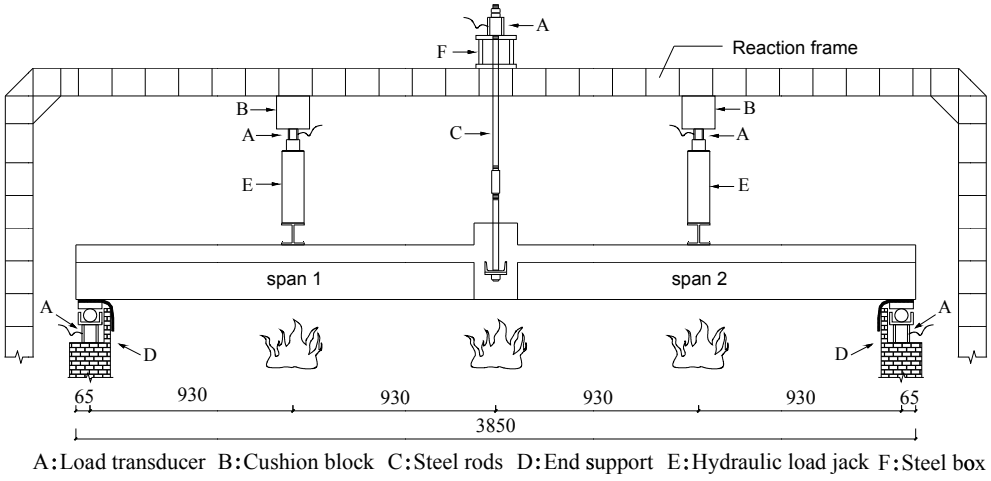

(a) test setup

(b) photo of test setup

(c) detail of middle support

Fig. 3. Test setup and transducer locations.

Table 2
Mechanical properties of reinforcement at ambient temperature.

Reinforcing bar grade	f_{yk} (N/mm^2)	f_{stk} (N/mm^2)
8 mm HPB300 (slab bars)	339.7	494.4
12 mm HRB335 (beam top bars)	368.6	540.0
12 mm HRB500 (beam bottom bars)	534.7	698.8

these locations during fire exposure and subsequent cooling. The load tests to failure following fire exposure were conducted using the same test arrangement (Fig. 3) but with a simple support beneath the middle (hogging) region of the beam; this is seen in subsequent Figures describing test results.

2.5. Temperature and strain measurement

During fire exposure, the three sides of the web and flange soffit of the continuous RC T-beam were exposed to fire. The top side of the beam flange was exposed to ambient conditions and the beam ends were insulated. Exploiting symmetry, temperature measurements were taken in only one span of the test beam. Fig. 5 shows the locations of thermocouples in each specimen. Nickel chromium alloy thermocouples, with a temperature range from −200 to 1100 °C, were used. As shown in Fig. 5, electrical resistance strain gauges were installed on the top and bottom CFRP sheets along one span for the tests to failure. Strain gauges were also located on the steel reinforcing bars of specimens GB1 and GB2.

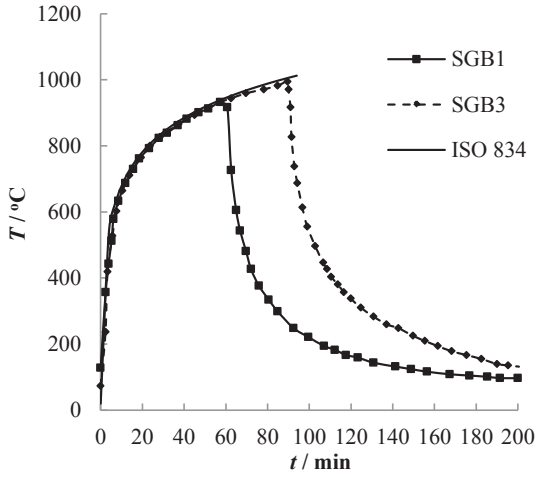

Fig. 4. Comparison between the measured furnace temperature and the ISO 834 standard fire curve.

3. Observations during fire exposure

Since all beams were essentially identical and subject to the same applied load, observations during the fire exposure was similar for each; only the observations from FGB3, having the longest exposure time (90 min), are presented here and shown in Fig. 6. Water vapour started to appear at 13 to15 minutes and did not stop until about 70 min into the fire exposure (Fig. 6a). The first hogging cracks developed about 200 mm from the middle support crossing the flange of the T-section about 9 to 10 min after fire exposure began as shown in Fig. 6c; these width of these cracks gradually increased with fire exposure time. At 70 min, multiple cracks were located between about 200 to 500 mm from the middle support crossing the flange. The width of these cracks ranged from 0.2 to 2.3 mm following 90 min fire exposure. Upon cooling the specimen, the crack widths decreased somewhat to range from 0.2 to 1.2 mm. Observations during fire exposure were consistent with those reported by Yu et al. [16] and Xu et al. [19] using similar specimens and test set-up.

3.1. Test specimen temperature development

Comparison between the measured furnace temperature and ISO 834 standard fire curve was shown in Fig. 4, highlighting a good agreement between the furnace temperature and ISO 834 standard fire curve. Fig. 7 presents the temperature development with time for specimens FGB2 and FGB3, having 60 and 90 min fire exposure, respectively. Temperature development in the SGB specimens was similar for specimens with the same exposure time. It can be seen that the temperature close to the surface of the concrete increases rapidly during the heating phase and decrease sharply once the fire was stopped. Internal temperatures increase slowly and continue to increase after the fire was stopped. Due to the effect of corner rounding and two-sided exposure, the temperature at the corner (measurement A1) was much higher than the temperature (measurement C1) at the same distance to the concrete surface at the flange. The temperature field in the flange plate was similar to that of a one-side fire exposed RC slab, and the temperature field of the web was similar to that of a three-side fire exposed RC rectangular beam.

3.2. Results of load tests to failure

The loading set-up used is shown in Fig. 3 and schematically in Fig. 8, in which for the experimental set-up $a = b = L/2$. Applied load versus sagging midspan deflection curves are shown in Fig. 9 and test key results are summarised in Table 3. The applied load is that applied

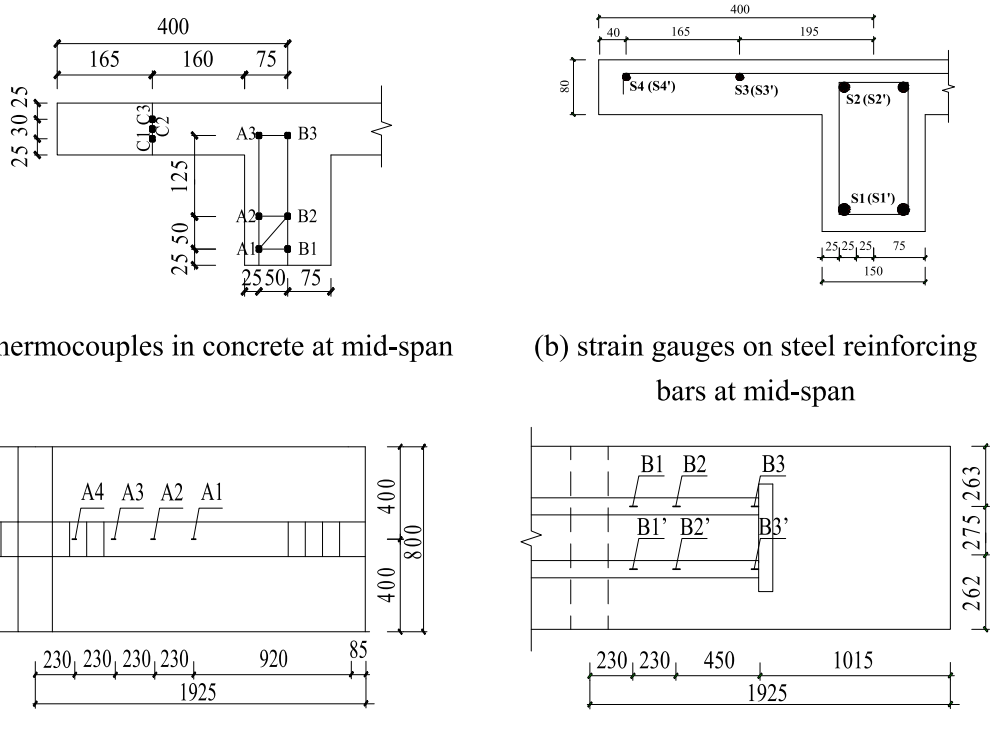

Fig. 5. Layout of thermocouples and strain gauges.

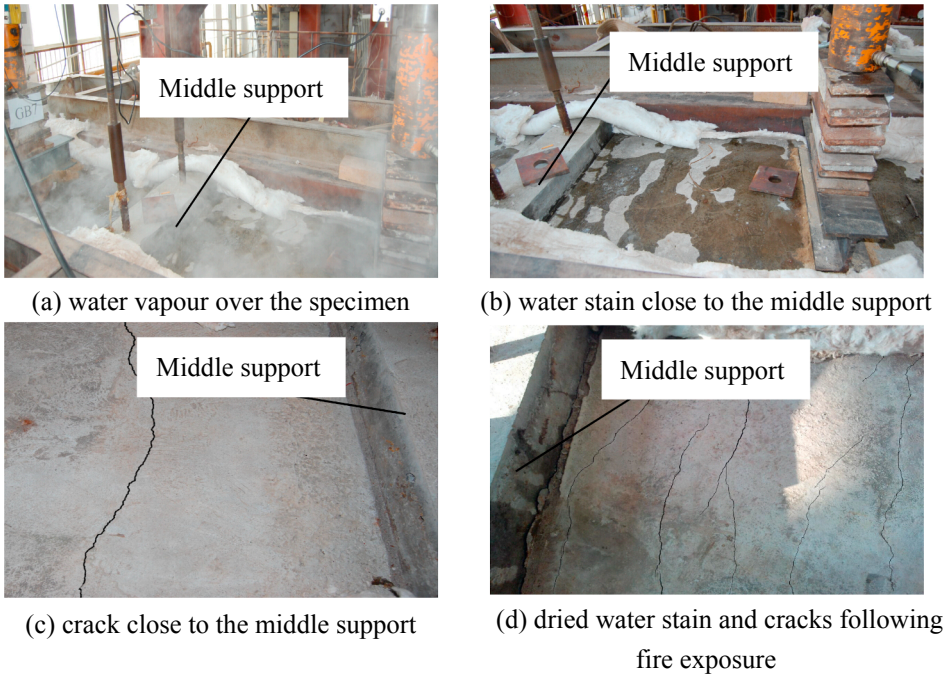

(a) water vapour over the specimen (b) water stain close to the middle support

(c) crack close to the middle support (d) dried water stain and cracks following fire exposure

Fig. 6. Test observations during fire exposure of specimen FGB3.

to one span (*P*) and the deflection reported is the average of that obtained at the midspan of each span. Some data for GB2 was lost; thus this specimen is not reported in Fig. 9.

The load-deflection curves illustrate both typical and expected behaviour. The relatively lightly reinforced control specimen (GB1) shows a gradually degrading stiffness and excellent ductility. Exposure to fire (FGB specimens) reduces both the stiffness and strength of the specimens but has little impact on the ability to achieve large deflections (although ductility falls). Finally, the addition of stiff EB-CFRP reinforcement – increasing the reinforcement ratio – results in increased capacity but reduced ductility. The specific behaviours are discussed at greater length in the following sections.

3.2.1. Tests to failure of control specimens GB1 and GB2

In the initial stage of the loading test, mid-span (sagging) deflection increased linearly with the applied load. Sagging cracks about 0.1 mm wide began to appear at the mid-span when the applied load on each span (*P* in Fig. 8) was 40 kN and 41 kN for GB1 and GB2, respectively. This load corresponds to the onset of non-linear load–deflection behaviour of the beams. When the applied load was about 68 kN and 67 kN for GB1 and GB2, respectively, hogging cracks, having a width of about 0.5 mm, appeared on both sides of the middle support. When the applied load was about 96 kN and 98 kN for GB1 and GB2, respectively, the hogging cracks at either side of the middle support extended through the flange of the T-section, having a width of 3.0 mm at the top surface. At applied loads of 134 kN and 139 kN for GB1 and GB2, respectively, concrete crushing was observed at the flange of the (sagging) mid-span section. Neither steel reinforcement rupture nor significant slip was observed in either beam indicating sufficient moment redistribution capacity to establish the ultimate plastic capacity of the beam. At failure, each span deformed into a V shape, as shown in Fig. 10, indicating the expected fully-plastic flexural failure mode. The ultimate applied loads (P_u) of GB1 and GB2 were 134 kN and 139 kN, respectively.

The strain data obtained from the internal reinforcing steel of specimen GB1 shown in Fig. 11 also confirm this interpretation of the behaviour of these beams. At an applied load of 96 kN the primary reinforcement in the flange of the T-section (S3 and S4 in Fig. 11a) exceeded its yield strain (approximately 2700 με) corresponding to the initial formation of the hogging region hinge. As seen in Fig. 9, the mid span deflection also began increasing at this stage as the internal forces are redistributed to the sagging moment region which retains some capacity; the bar strain at this stage in the sagging region (Fig. 11b) is approaching but remains below yield. As the applied load increased to about 104 kN, the primary reinforcement at the mid-span of the sagging region reached yield (S1 in Fig. 11b), indicating the formation of the second (and third) plastic hinge. Since concrete crushing ultimately controlled failure, the strain in the reinforcement at failure remained well below the fracture strain.

3.2.2. Tests to failure of fire-exposed specimens FGB2 and FGB3

Prior to testing to failure, FGB2 and FGD3 were exposed to the standard fire for 60 and 90 min, respectively. FGB2 exhibited severely damaged cover concrete to a depth of about 10 mm while FGB3 exhibited damage to a depth of about 25 mm. This damage was not repaired in any manner prior to testing to failure. Similar to the control beams GB1 and GB2, the deflection and the number of cracks in the sagging mid-span for specimens FGB2 and FGB3 gradually increased with the applied load, and primary cracks at mid-span and at the middle support (hogging) extend across through the whole section of the beam. A flexural failure mode was also observed for specimens FGB2 and FGB3. Fig. 12 shows the deformed shapes of specimens FGB2 and FGB3 following testing; the hinging at the middle support (hogging) and midspan (sagging) locations is clearly evident indicating a flexural failure and a sufficient degree of moment redistribution.

As summarised in Table 4, the stiffness and capacity of specimens FGB2 and FGB3 were markedly degraded following exposure to the standard fire. Initial flexural stiffness of FGB2 (60 min exposure) and FGB3 (90 min) was only 49% and 34%, respectively, of the stiffness of the control beams. The drop in both yield and ultimate capacities were less pronounced but also proportional to fire exposure time; residual ultimate capacity was 83% and 74% of the control beams for 60 and

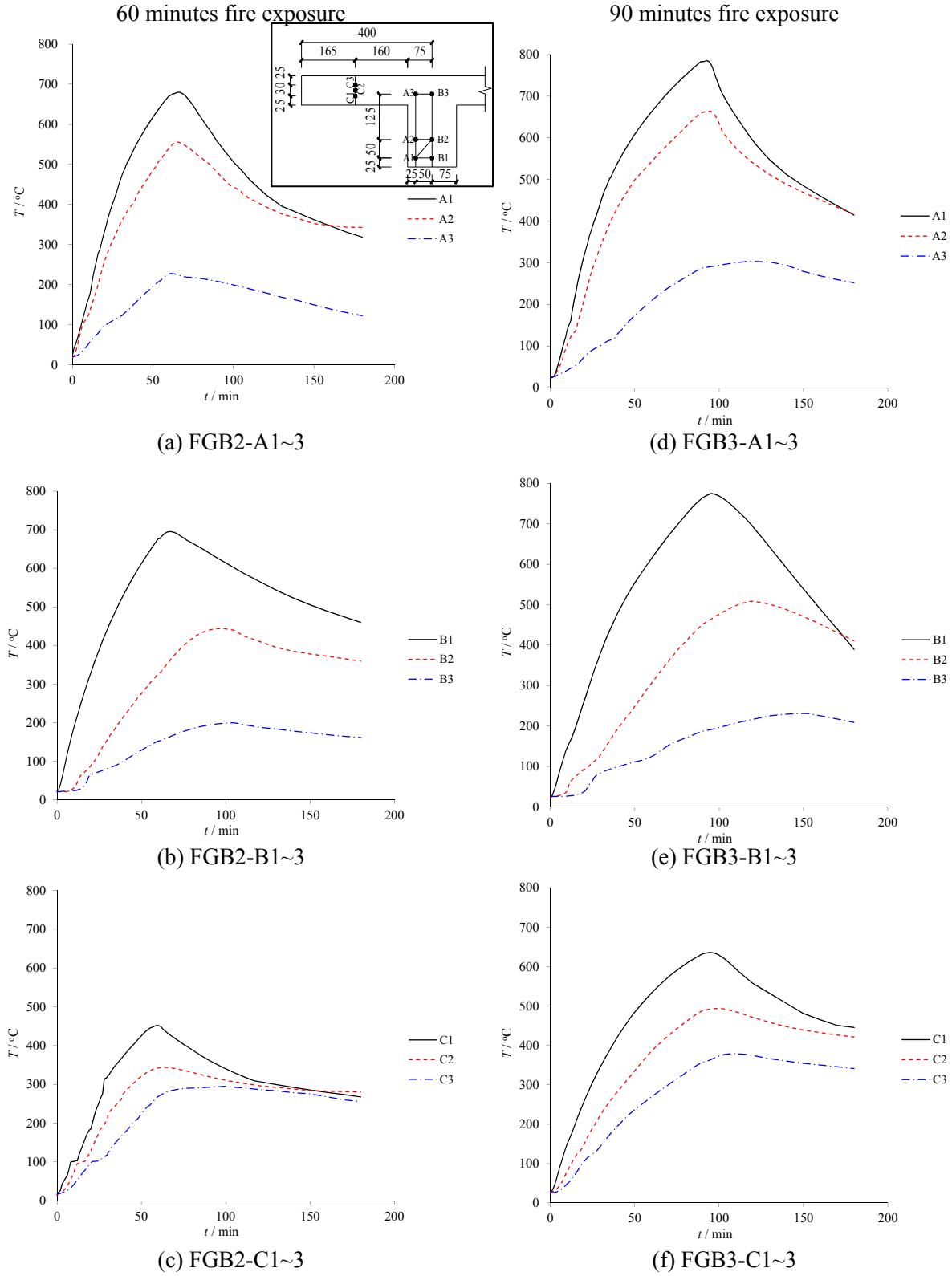

Fig. 7. Temperature development with time for thermocouples in FGB2 and FGB3.

90 min fire exposure, respectively.

Considering the temperature histories shown in Fig. 7, it is clear that the primary sagging reinforcing bars experienced temperatures approaching 700 °C and 800 °C, for 60 and 90 min fire exposure, respectively. More critically, the reinforcing bars were subject to prolonged exposure to temperature greater than 500 °C, followed by slow cooling. Such exposure would be expected to result in a degradation of steel properties. Specifically, following exposure to temperature less

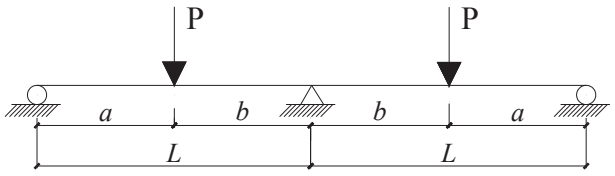

Fig. 8. Continuous beam loading arrangement.

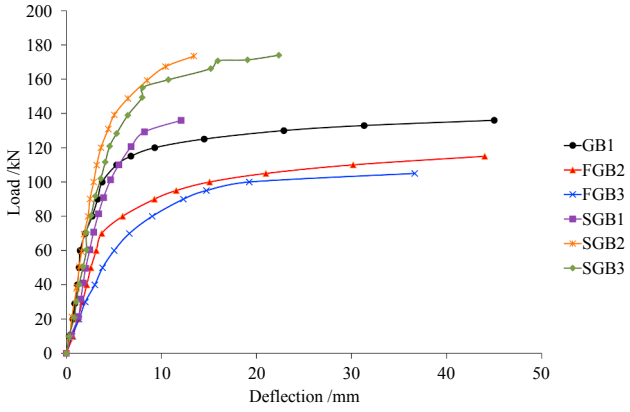

Fig. 9. Load-sagging midspan deflection curves for specimens.

than about 500 °C, the residual strength and modulus of steel reinforcing bar is mostly unaffected once the bar returns to room temperature [20]. However, following exposure to (and slow cooling from) temperatures exceeding about 700 °C, a residual effect on material properties resulting from microstructural changes in the steel is observed. For example, following exposure to and air-cooling from 800 °C, Neves et al. [21] report residual tensile strength of about 80% that at ambient and corresponding strains at rupture of about 140%. Additionally, the ratio between tensile and yield strength is known to approach 1 following exposure (and cooling) from 800 °C [22]. Nonetheless, residual modulus remains greater than 90% through exposure and cooling from as high as 1000 °C [22]. Temperature effects on the reinforcing bar material properties may be less significant than the effect of bond degradation[23]. While a complicated phenomenon, the degradation in capacity of FGB2 and FGB3 following fire exposure is believed to be typical of the exposures sustained.

3.2.3. Tests to failure of specimens SGB1-SGB3 repaired following fire exposure

The SGB specimens represent attempts to provide an EB-CFRP repair to specimens having their capacity degraded as FGB2 and FGB3, described above. It is assumed that the capacity of the existing steel reinforcement has degraded as a result of fire exposure and the EB-CFRP is intended to restore a portion of this lost capacity. Thus, in Table 4, the SGB specimens are compared to both the fire-damaged (FGB) and virgin (GB) specimens in terms of their ability to strengthen damaged beams and the degree to which the strengthening restores virgin capacity, respectively. For repaired specimens SGB1, SGB2 and SGB3, new cracks in the sagging region started to appear at an applied load of 40 kN. As the applied load increased, cracks extended from the web into the flange of the section in the sagging region. Failure of each SGB specimen was governed by failure of the EB-CFRP system applied implying that while effective, additional EB-CFRP than was used may have been more effective.

Specimen SGB1 (Fig. 13), having a single ply of EB-CFRP reinforcing the sagging regions exhibited rupture of the CFRP in both spans (Fig. 13b and c). As seen in Fig. 13a, the beam did not develop a plastic hinge mechanism (spans do not have a V shape) although a hinge likely developed in the hogging region. Since this region was not strengthened, the capacity of the beam was limited and did not exceed the capacity of the virgin GB beams (Table 3). This observation confirms that the EB-CFRP was inadequate to develop the available capacity of the strengthened beam by facilitating sufficient moment redistribution.

The behaviour of SGB2 (Fig. 14), identical to the SGB1 with the exception of additional reinforcement in the hogging region at the top of the flange, supports the hypothesized explanation of behaviour of SGB1. At failure, the EB-CFRP sheets in the hogging region of SGB2 ruptured (Fig. 14b) followed horizontal cracks developing at the bottom of both sagging mid-span sections (Fig. 14c). The horizontal cracking is interpreted as a bond failure driven by the sudden redistribution of moment associated with the brittle rupture of CFRP in the hogging region. Peeling failure of concrete cover along the reinforcement level was prevented by restraint provided by the U-strip anchors.

Specimen SGB3 (Fig. 15) behaved in a manner similar to SGB1 but achieved a greater capacity (Table 3) resulting from the additional CFRP used in the sagging region. In SGB3, the failure was characterised as rupture of the CFRP. Due to the significant energy released, following rupture a length of about 1.1 m of CFRP peeled away from the substrate (Fig. 15b). The plane of this failure passed through the first few mm of repair mortar (seen in Fig. 15b) indicating a good adhesive bond was achieved both between the CFRP and repair mortar and repair mortar and substrate concrete.

The strain distribution in the CFRP sheets along the span is shown in Fig. 16. The distribution with increasing load illustrates a typical pattern and indicates a sound bond. The *in situ* rupture strain is observed to be approximately 8000 με (Fig. 16 a, c and d), approximately 55% of the tensile test rupture strain. This value is somewhat lower than expected; *in situ* rupture strain of anchored CFRP is often observed to approach the tensile test rupture strain [4]. This may be attributed to the fact that the strain gauges did not record the maximum strain along the span of the CFRP sheets because of there may be stress

Table 3
Experimental results of all specimens.

Beam	Standard fire exposure time (min)	Initial bending stiffness, K (kN/m)	Yield load, P_y (kN)	Yield disp., Δ_y (mm)	Ult. load, P_u (kN)	Ult. disp., Δ_u (mm)	Ductility, Δ_u/Δ_y	Energy through yield E_y (J)	Energy through Ult. E_u (J)	Energy index E_u/E_y
GB1	0	38,980	104.0	8.91	134.0	45.37	5.09	502.7	4296.5	8.55
GB2	0	–	107.0	9.28	139.0	47.56	5.13	543.3	4651.2	8.56
FGB2	60	19,040	80.0	11.44	113.0	43.01	3.76	608.6	4074.5	6.70
FGB3	90	13,270	64.0	11.59	101.0	36.64	3.15	456.4	2701.9	5.92
SGB1	60	24,430	103.6	4.93	135.9	12.10	2.45	288.6	1200.6	4.16
SGB2	60	37,400	125.3	4.04	173.5	13.42	3.32	254.4	1597.6	6.28
SGB3	90	32,980	130.5	7.53	173.9	22.35	2.97	664.1	3467.9	5.22

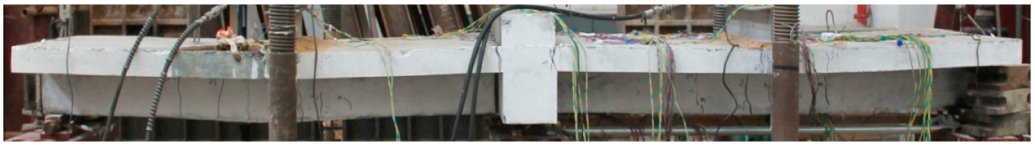

(a) GB1

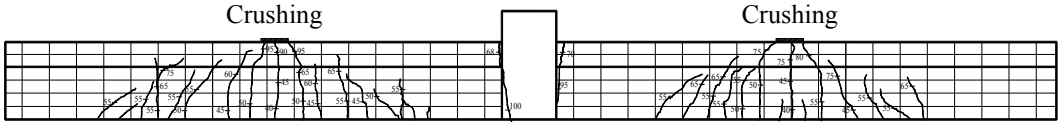

(b) crack distribution of GB1

(c) GB2

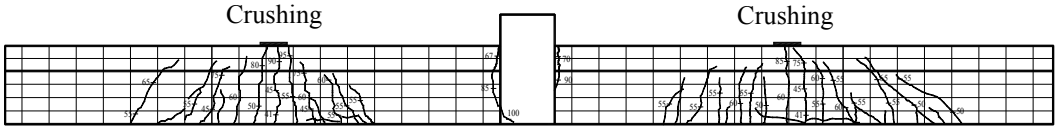

(d) crack distribution of GB2

Fig. 10. Failure mode and crack pattern of control specimens GB1 and GB2.

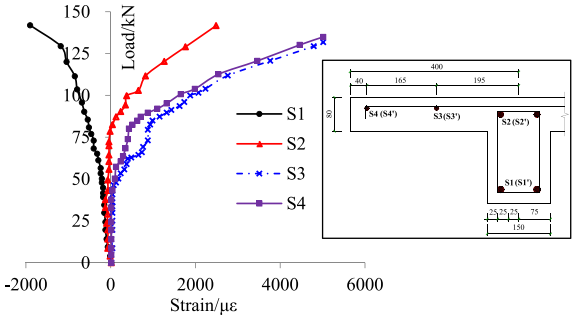

(a) middle support section

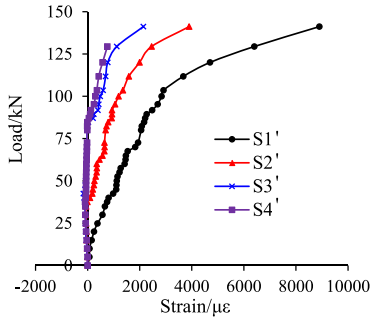

(b) mid-span section

Fig. 11. Developments of steel reinforcement strains of GB1.

concentration on the CFRP sheets and the limitation of the static data log system employed. In the sagging region of SGB2 where no debonding or rupture was observed, the CFRP strains only achieved about 6000 με indicating some reserve capacity likely remained at this location.

As reported in Table 3, the EB-CFRP retrofit measures of both SGB2 and SGB3 successfully restored the virgin capacity of the beam and were sufficient to also restore most of the lost initial stiffness.

4. Discussion of results and analysis

Table 4 provides ratios of specimen response normalised by both control specimens (1/GB) and the fire-exposed specimen having the same exposure time (1/FGB). Test parameters obtained from the load deflections responses – stiffness and yield and ultimate capacities – have already been discussed.

Two measures of ductility that have been used in previous studies of continuous beams [5,6] were calculated and are reported in Table 3. Displacement ductility is the ratio of deflection at ultimate capacity to that at yield: Δ_u/Δ_y. The "energy ductility" is the ratio of energy absorbed by the beam at ultimate capacity to that at yield: E_u/E_y. The values of energy are determined as the area under the load deflection curve up to yield or ultimate capacity. Although the values are different, the trends in measures of ductility are similar. A loss of ductility is observed following exposure to fire. The process of strengthening increases the reinforcing ratio which results in a further loss in ductility.

4.1. Moment redistribution

From the reaction forces measured during testing, the sagging and hogging moments were calculated as shown in Fig. 17 and Table 5. These were compared with the same moments calculated from an elastic analysis assuming uniform flexural stiffness along the span (Fig. 8). For control specimen GB1, at the early stages of loading, the measured sagging and hogging moments were close to those calculated

(a) FGB2

(b) FGB3

Fig. 12. Failure mode of unstrengthened fire-damaged specimens FGB2 and FGB3.

Table 4
Effects of fire damage (1/FB) and subsequent repair (1/FGB).

Beam	Standard fire exposure time (min)	Initial stiffness, K		Yield load, P_y		Ult. load, P_u		Ductility, Δ_u/Δ_y		Energy index E_u/E_y	
		1/GB	1/FGB	1/GB	1/FGB	1/GB	1/FGB	1/GB	1/FGB	1/GB	1/FGB
FGB2	60	0.49	–	0.76	–	0.83	–	0.74	–	0.78	–
FGB3	90	0.34	–	0.61	–	0.74	–	0.62	–	0.69	–
SGB1	60	0.63	1.28	0.98	1.30	1.00	1.20	0.48	0.65	0.48	0.62
SGB2	60	0.96	1.96	1.19	1.57	1.27	1.54	0.65	0.88	0.73	0.94
SGB3	90	0.85	2.49	1.24	2.04	1.27	1.72	0.58	0.94	0.61	0.88

(a) deformed shape

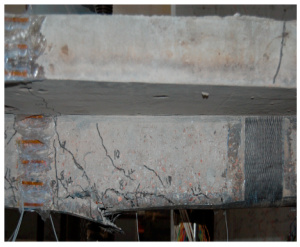

(b) tensile rupture of CFRP at left mid-span

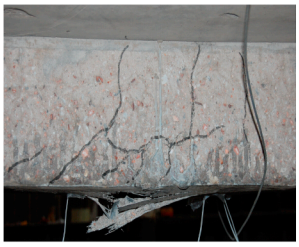

(c) tensile rupture of CFRP at right mid-span

(d) cracks near middle support

Fig. 13. Failure mode of specimen SGB1.

from elastic analysis, indicating a nearly elastic behaviour of the continuous RC T-beams. As the load increases, the concrete cracks and eventually the steel reinforcement yields. The measured sagging and hogging moments gradually diverged from those calculated by elastic analysis since the beam behaviour is no longer elastic and its stiffness is no longer uniform along the spans. As the load increases, moment redistribution between regions of the continuous beam may develop. At failure, the hogging moment is greater than the elastic predictions, while the sagging moment is lower. This may be explained by the fact that the stiffness of the beams in the sagging moment region degraded faster than that in the hogging moment region. As seen in Figs. 10, 12–15, the extent (number, width and distribution) of cracking in the sagging regions was more significant that in the hogging region.

For strengthened specimens SGB1, SGB2 and SGB3, on the other hand, the hogging moments are mostly lower than the elastic predictions, while the sagging moments are mostly higher, even when the

(a) deformed shape

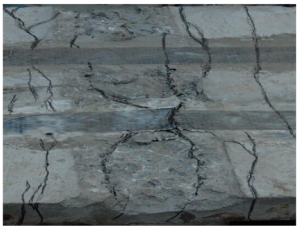

(b)tensile rupture of top CFRP over middle support

(c) horizontal crack at left mid-span

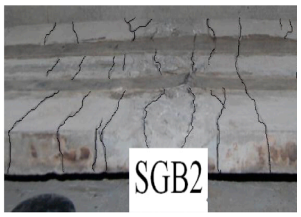

(d) cracks near middle support

Fig. 14. Failure mode of specimen SGB2.

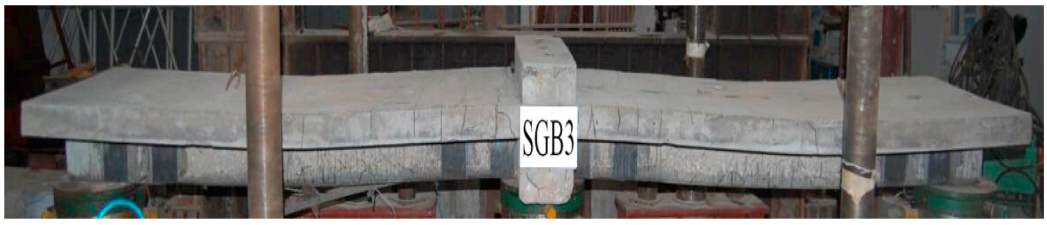

(a) deformed shape

(b) peeling off of CFRP at left mid-span

(c) cracks at the mid-span

(d) cracks near middle support

Fig. 15. Failure mode of specimen SGB3.

load was small. This may be partially attributed to the variation of the flexural stiffness along the beam span resulting from fire exposure. In the hogging region, the compressive region of cross section was exposed directly to fire, while in the sagging region, the tensile region was exposed. Concrete cracking and fire-induced material degradation lead to varying stiffness along the span. The change in behaviour of SGB from GB specimens also reflects the repair involved. Although modest, each EB-CFRP ply increased the equivalent steel reinforcing ratio, ρ, 0.0009 (about 14%). Since the beam remains under-reinforced, the capacity of the beam at this location – and the cracked stiffness will increase, affecting the moment redistribution.

The moment redistribution ratio, β, given in Table 5 was calculated for the hogging bending moment. The redistribution ratio reflects the moment redistribution capacity of the continuous beams calculated as: $(M_e - M_m)/M_e$, where M_m is the bending moment from experiments determined from measured boundary reactions, and M_e is the bending moment calculated from an elastic analysis. A negative value indicates moment being redistributed from the sagging to the hogging region (GB) and a positive value indicates redistribution from the hogging to the sagging. The change in redistribution 'direction' for SGB1 and SGB3 – both only strengthened in the sagging region – demonstrate the efficacy of this strengthening technique. In SGB2, the addition of hogging region CFRP strengthened the beam but minimised the ability to redistribute moments by making the capacities of the regions similar. The measured boundary reactions for GB2, FGB2 and FGB3 were not recorded.

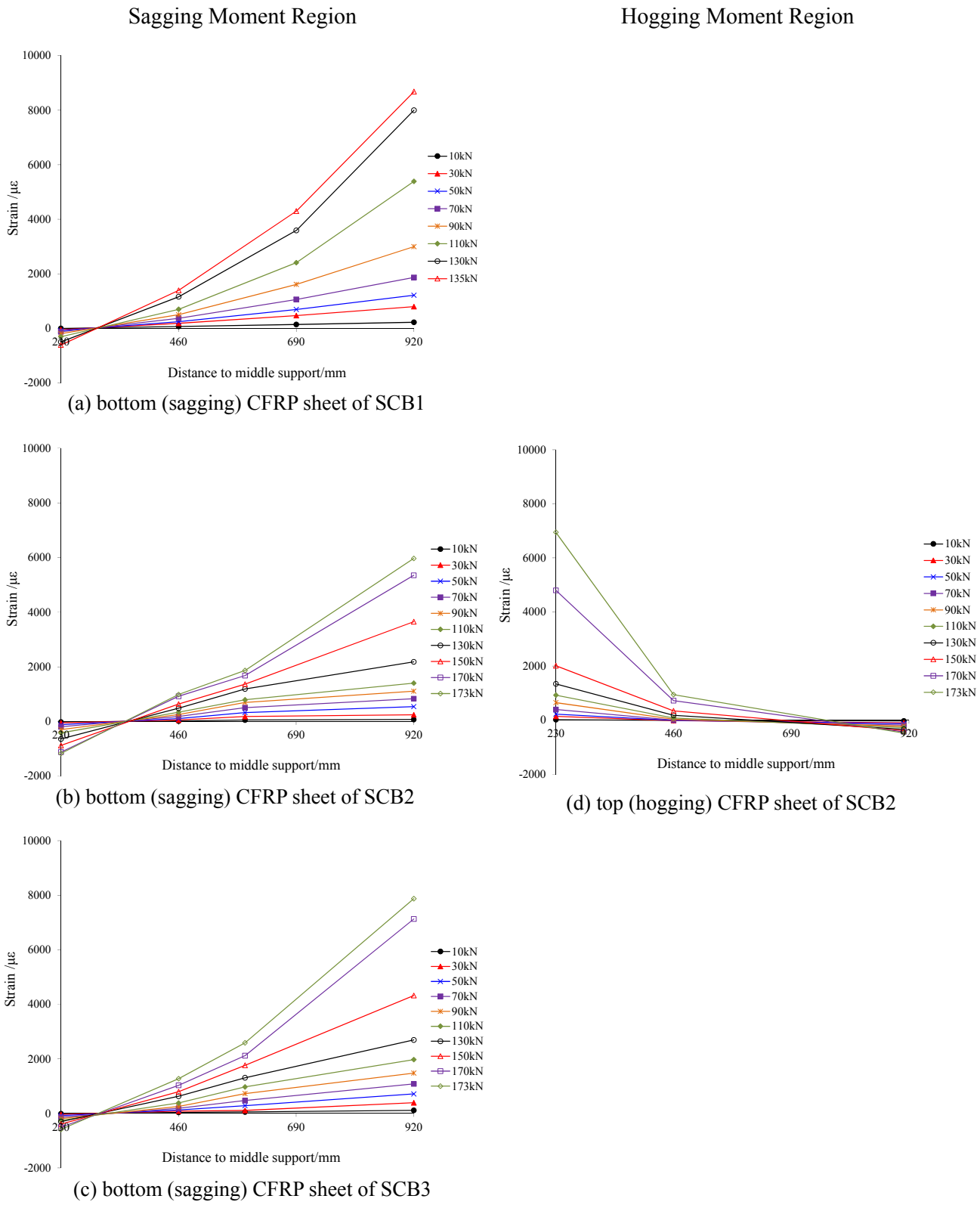

Fig. 16. Strain distribution of CFRP sheets along beam span.

4.2. Prediction of the load capacity

The residual moment capacity of fire-damaged continuous RC T-beam may be calculated using the 500 °C isotherm method suggested in EC 2 [1], with the material property of steel reinforcement replaced with its material property following fire exposure. The strength of all concrete experiencing temperature greater than 500 °C is taken as zero; concrete not experiencing 500 °C is assumed to be unaffected and properties are those at room temperature. The section moment capacity is then calculated based on the plane section assumption and the 500 °C isotherm method. The strain, stress and forces on the section with and without CFRP sheets are illustrated in Fig. 18. The neutral axis depth is

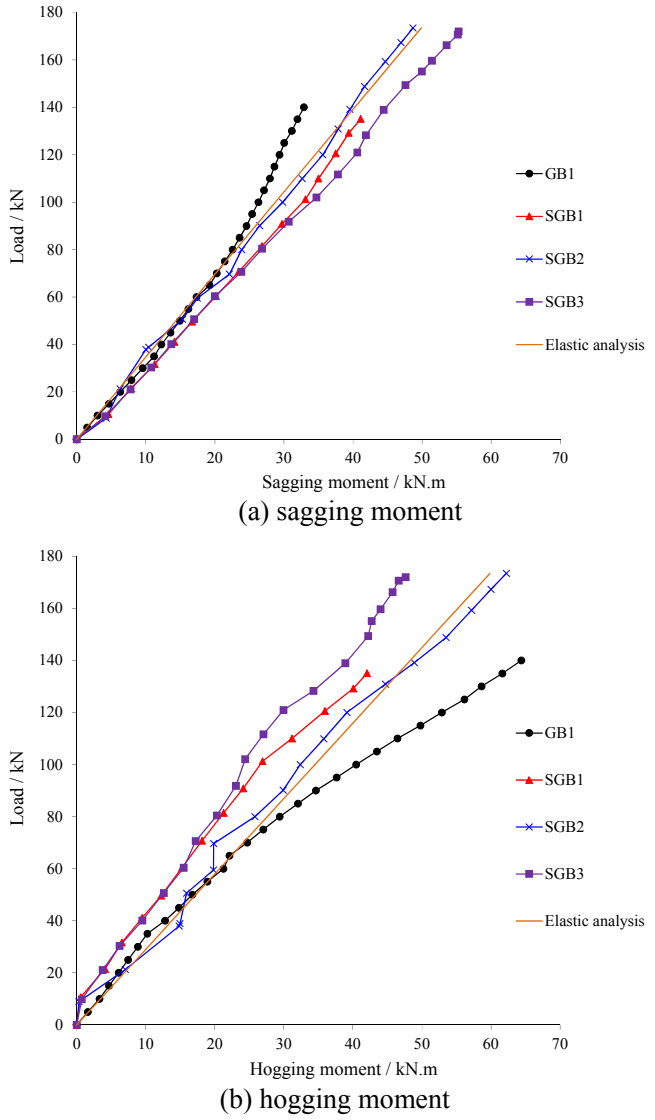

Fig. 17. Comparison of sagging and hogging moments from experiment and elastic analysis.

initially assumed and the correct value is determined iteratively when the equilibrium of internal forces is satisfied. Failure criteria in the sagging and hogging moment section is assumed to be tensile rupture of CFRP sheets and concrete crushing respectively. For the continuous beam shown in Fig. 8, the value of the applied load P can be calculated as:

$$P = \frac{LM_{sag} + aM_{hog}}{a(L-a)} \quad (1)$$

where L is the length of a single span; a is the distance of applied load to the end simple support; M_{sag} is the moment capacity at the mid span of the sagging region and M_{hog} is the moment capacity at the hogging region.

It is assumed that both the sagging and hogging sections have sufficient ductility to permit a plastic hinge mechanism to develop when the beam reaches its flexural capacity. In this study, however, specimen SGB2 strengthened with EB-CFRP in both the sagging and hogging regions, was unable to develop both hinges due to the brittle nature of CFRP sheet rupture. Therefore, the proposed method was unable to predict the capacity of this member. The resulting predictions of specimen ultimate capacity are given in Table 5 and shown to predict the experimental capacity with reasonable precision.

5. Conclusions

This paper has presented the results of an experimental study to investigate the performance of fire-damaged continuous reinforced concrete (RC) T-beams strengthened with EB-CFRP sheets. In total, seven tests were carried out including two tests conducted on control specimens not exposed to fire and five tests on beams first exposed an ISO 834 standard fire for either 60 or 90 min. Of the fire-exposed tests, two were tested to failure following fire exposure and three were repaired with EB-CFRP and tested to failure. The following conclusions have been drawn:

(1) The unexposed control beams (GB1 and GB2) behaved in a flexural manner. Damage was concentrated in the sagging region and significant moment redistribution (30%) toward the hogging region was exhibited. This behaviour is typical of under-reinforced continuous RC T-beams.
(2) The stiffness and capacity of fire-damaged specimens (FGB2 and FGB3) were markedly degraded following exposure to the standard fire. Initial flexural stiffness of FGB2 (60 min exposure) and FGB3 (90 min) was only 49% and 34%, respectively, of the stiffness of the control beams. The drop in both yield and ultimate capacities were less pronounced but also proportional to fire exposure time; residual ultimate capacity was 83% and 74% of the control beams for 60 and 90 min fire exposure, respectively.
(3) The EB-CFRP strengthening of fire damaged beams was shown to mostly mitigate the effects of fire exposure. The EB-CFRP retrofit measures of both SGB2 and SGB3 successfully restored the virgin capacity of the beam and were sufficient to also restore most of the lost initial stiffness. Because CFRP retrofit increases the reinforcing present, the increase in stiffness and strength is accompanied by a further loss of ductility.
(4) While not the focus of the study, the role of anticipated moment redistribution is highlighted. The CFRP-strengthened beams exhibited moment redistribution from the strengthened sagging region to the hogging region (SGB1 and SGB3) demonstrating the efficacy of this strengthening technique. In SGB2, the addition of hogging region CFRP strengthened the beam but minimised the

Table 5
Moment redistribution and strength predictions of all specimens.

Beam	Standard fire exposure time (min)	Hogging bending moment (kN·m)			Predicted capacity, P (kN)		
		Elastic analysis	Measured	Redistribution factor, β	Measured	Predicted	Measured predicted
GB1	0	47.0	61.0	−0.30	134.0	132.7	1.01
GB2	0	48.7	–	–	139.0	132.7	1.05
FGB2	60	39.6	–	–	113.0	106.5	1.06
FGB3	90	35.4	–	–	101.0	101.7	0.99
SGB1	60	47.6	42.1	0.12	135.9	131.5	1.03
SGB2	60	60.8	62.2	−0.02	173.5	155.9	1.11
SGB3	90	61.0	47.6	0.22	173.9	171.7	1.01

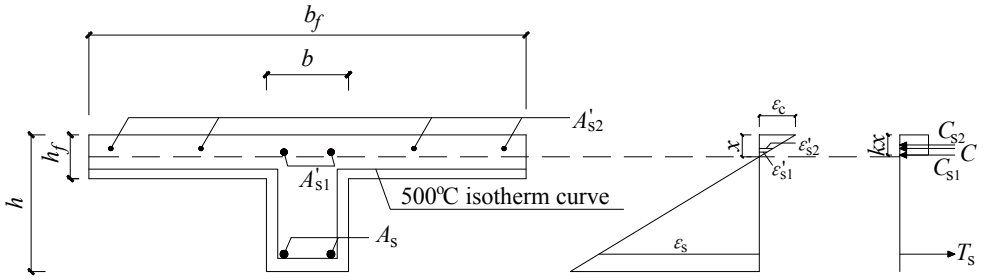

(a) sagging moment section

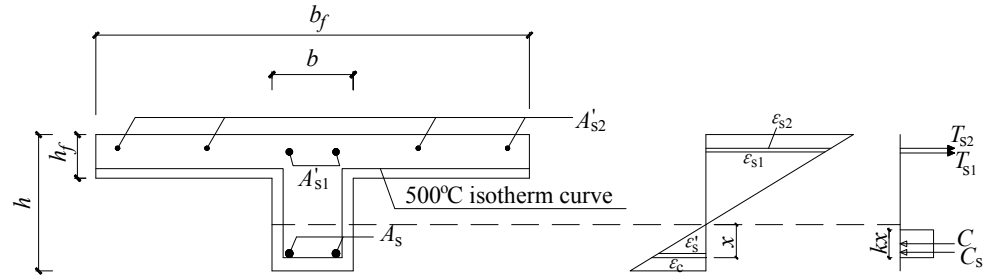

(b) hogging moment section

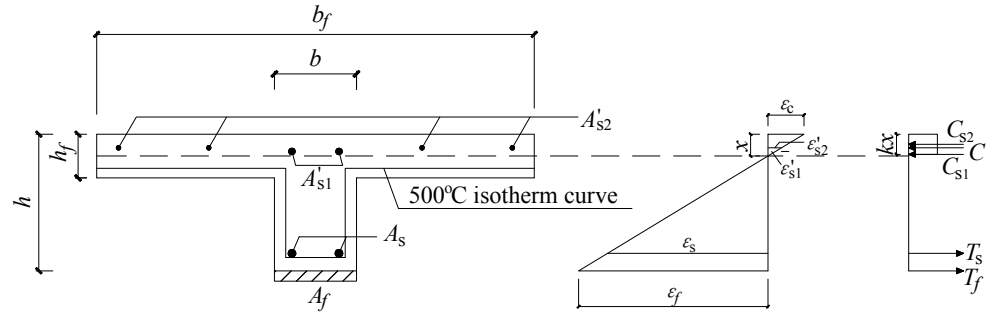

(c) sagging moment section with CFRP sheets

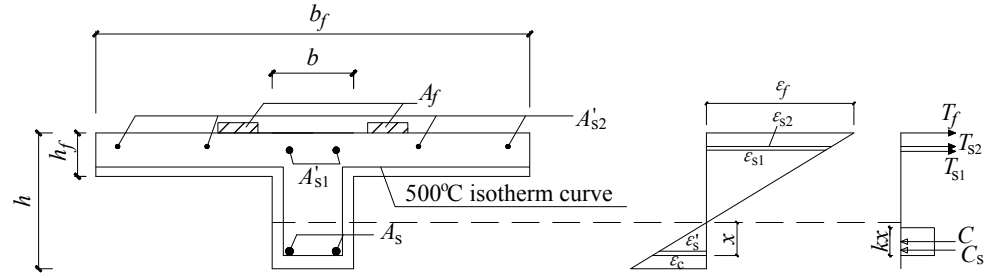

(d) hogging moment section with CFRP sheets

Fig. 18. Strain, stress and forces on the section without and with CFRP sheets.

ability to redistribute moments by making the capacities of the regions similar.

(5) Simple prediction using plane sections analysis and the assumptions of the 500 °C isotherm method [1] were shown to accurately predict the behaviour of the fire-damaged specimens.

Acknowledgement

This work was financially supported by the National Key R&D Program of China (Grant No. 2016YFC0701306), the Standard Program of Shanghai Science and Technology Commission (No. 17DZ2202600).

References

[1] EN1992-1-2. Eurocode 2: Design of concrete structures -Part 1-2: General rules – Structural fire design. British Standard Institution. Brussels: European Committee for Standarization; 2004.

[2] El-Hawary MM, Ragab AM, El-Azim AA, Elibiari S. Effect of fire on flexural behaviour of RC beams. Constr Build Mater 1996;10(2):147–50.

[3] Teng JG, Chen JF, Smith ST, Lam L. FRP:strengthened RC structures. Chichester (UK): John Wiley & Sons, Ltd; 2001.

[4] ACI 440.2R-17. Guide for the design and construction of externally bonded FRP systems for strengthening concrete structures. Farmington Hills (MI, USA): American Concrete Institute; 2017.
[5] Ashour AF, El-Refaie SA, Garrity SW. Flexural strengthening of RC continuous beams using CFRP laminates. Cem Concr Compos 2004;26(7):765–75.
[6] El-Refaie SA, Ashour AF, Garrity SW. Sagging and hogging strengthening of continuous reinforced concrete beams using carbon fiber-reinforced polymer sheets. ACI Struct J 2003;100(4):446–53.
[7] Aiello MA, Valente L, Rizzo A. Moment redistribution in continuous reinforced concrete beams strengthened with carbon-fiber reinforced polymer laminates. Mech Compos Mater 2007;43(5):453–66.
[8] Aiello MA, Ombres L. Moment redistribution in continuous fiber-reinforced polymer-strengthened reinforced concrete beams. ACI Struct J 2011;108(2):158–66.
[9] Akbarzadeh H, Maghsoudi AA. Flexural strengthening of RC continuous beams using hybrid FRP sheets. The 5th International Conference on FRP Composites in Civil Engineering, Beijing, China. 2010.
[10] Kumar PU, Raju MP, Rao KS. Performance of repaired fire affected RC beams. Curr Sci India 2009;96(3):398–402.
[11] Haddad RH, Shannag MJ, Moh'd A. Repair of heat-damaged RC shallow beams using advanced composites. Mater Struct 2007;41(2):287–99.
[12] Haddad RH, Al-Mekhlafy N, Ashteyat AM. Repair of heat-damaged reinforced concrete slabs using fibrous composite materials. Constr Build Mater 2011;25(3):1213–21.
[13] Irshidat MR, Al-Saleh MH. Flexural strength recovery of heat-damaged RC beams using carbon nanotubes modified CFRP. Constr Build Mater 2017;145:474–82.
[14] Jumaat MZ, Rahman MM, Alam MA. Flexural strengthening of RC continuous T beam using CFRP laminate: a review. Int J Phys Sci 2010;5(6):619–25.
[15] Xiang K, Wang GH, Zhao T, Lu ZD. Experiment and analysis of CFRP strengthened fire-damaged reinforced concrete continuous T-beams. Procedia Eng 2011;11:541–9.
[16] Yu JT, Liu Y, Lu ZD, Xiang K. Experimental Study on damage and rehabilitation of reinforced concrete continuous member after fire. J Tongji Univ (Nat Sci) 2012;40(4):508–14.
[17] GB 50010-2010. Code for design of concrete structures. Beijing: China Architecture & Building Press; 2010.
[18] ISO834-11:2014. Fire resistance tests – elements of building construction – Part 11: Specific requirements for the assessment of fire protection to structural steel elements. Geneva: International Organization for Standardization; 2014.
[19] Xu Q, Han C, Wang YC, Li X, Chen L, Liu Q. Experimental and numerical investigations of fire resistance of continuous high strength steel reinforced concrete T-beams. Fire Safety J 2015;78:142–54.
[20] Kodur VKR, Agrawal A. An approach for evaluating residual capacity of reinforced concrete beams exposed to fire. Eng Struct 2016;110:293–306.
[21] Neves IC, Rodrigues JPC, Loureiro AP. Mechanical properties of reinforcing and prestressing steel after heating. J Mater Civil Eng 1996;8(4):189–94.
[22] Tao Z, Wang X-Q, Uy B. Stress-strain curves of structural and reinforcing steels after exposure to elevated temperatures. J Mater Civil Eng 2013;25(9):1306–16.
[23] Kodur VKR, Agrawal A. Effect of temperature induced bond degradation on fire response of reinforced concrete beams. Eng Struct 2017;142:98–109.